JOURNAL OF SPACECRAFT AND ROCKETS
Vol. 39, No. 5, September–October 2002

Design Study of a Square Solar Sail Architecture

G. Greschik* and M. M. Mikulas†
University of Colorado, Boulder, Colorado 80309-0429

The impact on the achievable performance and some key structural characteristics in 100-m square solar sails of various design conditions and parameters is explored. Upper-bound performance is addressed with an architecture of manageable mechanics and likely ultimate structural efficiency in this class of sails due to uniaxial tensioning in each quadrant, namely, the stripped sail. The designs are performed with a limit point friendly approach. These innovations are justified by reviewing response fundamentals including sail billow, boom mechanics, and operational failure modes. The observations and conclusions advance the state of the art in sail design and provide guidance for future engineering.

Nomenclature

a_c	=	characteristic acceleration, mm/s^2
b	=	square sail edge length, m
d	=	tubular boom diameter, $2r$, cm
E	=	boom wall Young's modulus, GPa
F	=	axial boom cross section force, N
L	=	boom length, m
l	=	strip length, m
m_{tot}	=	entire spacecraft mass, kg
m_{4b}	=	mass of all four booms, kg
p	=	pressure, Pa
R_{Eu}	=	global (Euler) buckling safety coefficient
r	=	tubular boom radius, cm
t	=	film thickness, μm
t_b	=	boom wall thickness, mm
δ	=	sag (billow), m
ε	=	engineering strain
η	=	efficiency of specular reflectivity
ξ	=	normalized catenary sag, δ_c/b
$\bar{\rho}$	=	structural surface density (structural mass per area), kg/m^2
σ	=	film skin stress, Pa, kPa, psi

Introduction

The Prevailing vs the Present Design Paradigm

THERE are many solar sail concepts available.[1–3] (See also popular illustrations.[4]) For simplicity and deployability, near- and medium-term design efforts tend to focus singularly on the unrigged square sail,[5] where a square film is supported by four simple diagonal booms. Furthermore, attention is mostly paid to the four- and five-point suspension variants of this concept (Figs. 1a–1c).

For a preliminary design addressing no attitude variations, trajectory analysis, and nonlinear orbital dynamics, the boom loads are typically calculated from 1) the light pressure, 2) the boom inertial loads from the acceleration by the propulsion, and 3) the required film tension as defined by assumptions according to the (projected) state of the art on film reflectivity, wrinkles, and material properties. Next, the boom global and local stability margins are compared with comfortably large limits (typically $R_{\text{Eu}} \geq 1.5$ for Euler buckling). The boom lateral deformations are usually calculated from the lateral loads alone, without accounting for the nonlinear beam-column effect by compression. (This approximation is acceptable only when the margin of safety R_{Eu} against global buckling is large. If $R_{\text{Eu}} = 4$, the deformations calculated from the lateral loads are still underestimated approximately 25%.)

This common design scenario is based on linear theory and assumes that, the wider the margin between the theoretical Euler buckling load and the actual axial loads, the safer the design. This fundamental premise is reviewed and abandoned in the present work. Linear theory is abandoned, and design is based on a geometrically nonlinear beam-column analysis to 1) allow for the rational and accurate assessment of boom responses near the theoretical Euler buckling load; 2) permit sensitivity studies; 3) accommodate any boom construction, taper, load type, and distribution; and 4) allow shaped (nonflat) sails.

To avoid bias toward any one configuration and to render the analysis of the complex sail billow problem manageable, the traditional focus on four- and five-point sail suspension is also abandoned. Instead, attention is directed to an architecture with a high potential of ultimate efficiency, originally conceived by the paper's second author and herein termed the stripped design (Fig. 1e). Neither technological feasibility nor infeasibility is implied.

Novelty and Significance

The nonlinear beam-column boom design and the stripped architecture dramatically depart from the prevailing sail design paradigm. However, the contributions are not limited to using a nonlinear design approach and proposing an upper bound architecture. The two combined reduce the structural overhead significantly, as demonstrated with a design study.

Characteristic accelerations $a_c \approx 1$ mm/s^2 are achieved with $t = 2.5$ μm $= 0.1$ mil sail film, $\sigma = 6.9$ kPa $= 1$ psi skin stress, $\eta = 0.85$ specular reflectance, and $E = 6.9$ GPa $= 10^7$ psi tubular boom wall material stiffness for 100- and 400-m sails carrying 20- and 320-kg payloads, respectively. Uniform boom cross sections for the 100-m designs have $d = 5$–7.5 cm $= 2$–3 in. diameters for $t_b = 0.10$–0.25 mm $= 4$–10 mils wall thicknesses (Fig. 2). For the similarly efficient 400-m designs, the boom diameters vary $d = 22.5$–30 cm $= 8.5$–12 in. for the same wall thickness range (Fig. 3, compared later). (The total mass m_{tot} shown includes all components, sail, booms, payload, overheads, etc., whereas the structural surface density $\bar{\rho}$ only accounts for the sail and boom masses.)

Beyond illustrating point designs and demonstrating parametric trends, key conclusions on general sail design are also reached. The need for constant force sail suspension mechanism is highlighted, and some engineering issues are touched on, including failure modes.

Software Tools

This work was aided by two first-generation spreadsheet programs: SqS (Square Sail) for the fully nonlinear interactive design and analysis of square solar sails and Elastica, a general

Received 5 July 2001; revision received 28 February 2002; accepted for publication 18 April 2002.

*Research Associate, Department of Aerospace Engineering Sciences, Center for Aerospace Structures, C. Box 429, UCB 429; greschik@colorado.edu. Member AIAA.

†Professor Emeritus of Aerospace Engineering, Department of Aerospace Engineering Sciences, Center for Aerospace Structures, C. Box 429, UCB 429; mikulas@colorado.edu. Fellow AIAA.

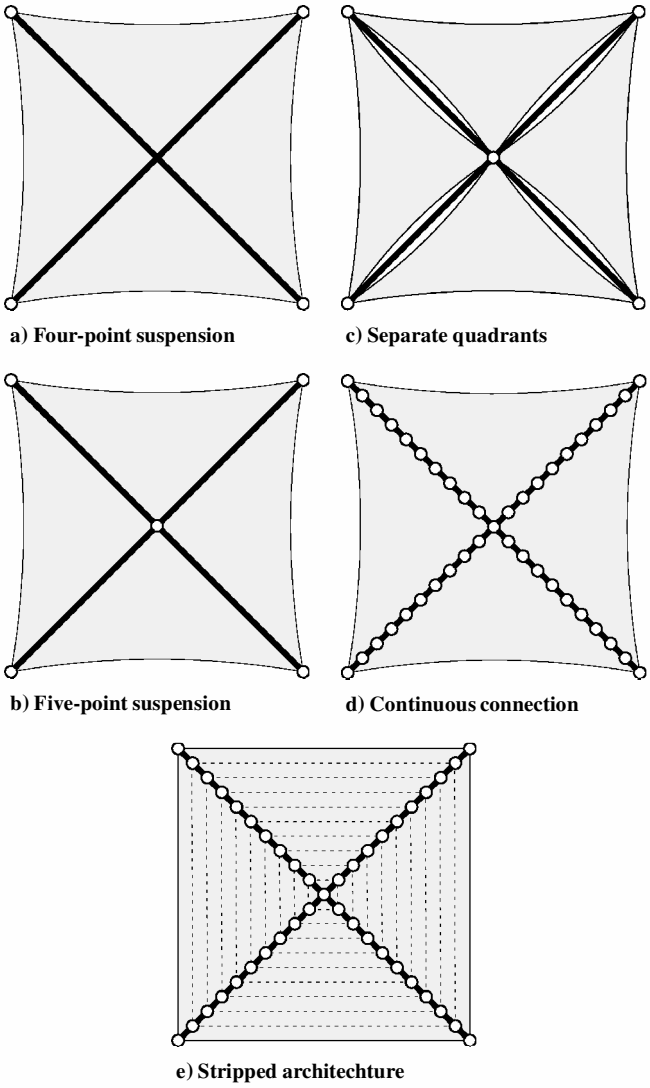

Fig. 1 Some square sail suspension patterns: ○, sail suspension from boom; ——, sail surface edge; - - - -, strip borders/stress direction; and ——, boom.

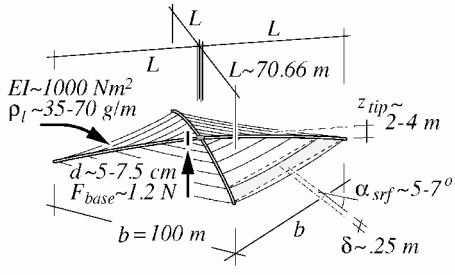

Fig. 2 Parameters for 100-m stripped sails at 1 AU: payload, m_{pl} = 20 kg; sail film, σ_{skin} = 6895 Pa = 1 psi; t = 2.5 μm; sailcraft, m_{tot} ~ 75–85 kg; $\bar{\rho}$ ~ 5.3–5.9 g/m²; and performance, a_c ~ 0.9–1 mm/s².

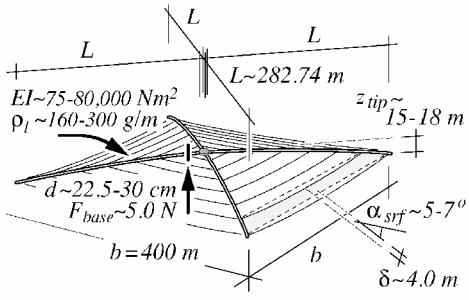

Fig. 3 Parameters for 400-m stripped sails at 1 AU: payload, m_{pl} = 320 kg; sail film, σ_{skin} = 6895 Pa = 1 psi; t = 2.5 μm; sailcraft, m_{tot} ~ 1200–1350 kg; $\bar{\rho}$ ~ 5.4–6.3 g/m²; and performance, a_c ~ 0.9–1 mm/s².

beam-column analysis tool to model elastic cantilevers with unusual loading conditions. Both programs involve sophisticated numerics and interactive features for the automatic execution and manual control of nonlinear boom shape integration and the calculation of boom loads.

To calculate properly the boom loads for the stripped design, SqS keeps track of the three-dimensional geometry of film strip billows and orientations as they depend on the curved boom shape. Nonlinear aspects of film reflection and the inertial loads arising from sailcraft acceleration are also accounted for.

Key Assumptions

To offer guidelines and contribute to quantifying upper bound performance (as opposed to proposing engineering solutions), we rely on a number of assumptions, some of which are based on engineering forecast. Namely, we assume that 1) sufficient reflectivity can be ensured with a uniaxial skin stress of ≈6.9 kPa, 2) fabrication and deployment will be possible, 3) imperfections and thermal effects can be controlled, 4) dynamic responses (to orbital and environmental conditions, postdeployment effects, etc.) can be sufficiently controlled to allow vibrational and wave dynamics to be ignored in preliminary design, and 5) all other technical challenges can also be overcome.

Stripped Architecture

Mechanical Characteristics

The global boom mechanics critically depends on the load path through which the booms, via axial compression, channel sail tension to their bases. The collectively shortest load path from all film surface points corresponds to uniaxial tension in each quadrant parallel to the square edge with continuous suspension along the booms, namely, the stripped configuration (Fig. 4). This scheme, thus, represents the best achievable performance among like sails as illustrated via the comparison of boom loading for a few configurations in Fig. 5 (where the distributed load q by the stripped sale is taken uniform for reasons discussed in the next major section). For the Fig. 5d case (outboard and side catenaries for a sail of four quadrants), all catenary arc radii are chosen equal. The approximate expressions for F_{base} (shown in terms of the reference base load $F_0 = \sigma t L$ and the normalized outboard catenary sag $\xi = \delta_c/b$) correspond to shallow catenary arcs, $\xi \ll 1$, when the arc end slopes are negligible. This condition is critical because the effects of these slopes remain significant even when the overall arc shapes already resemble the straight square sail edges. The errors due to ignoring the end slopes are nonconservative, as shown in Table 1 for the approximate relations in Fig. 5. Note also that these errors, as well as

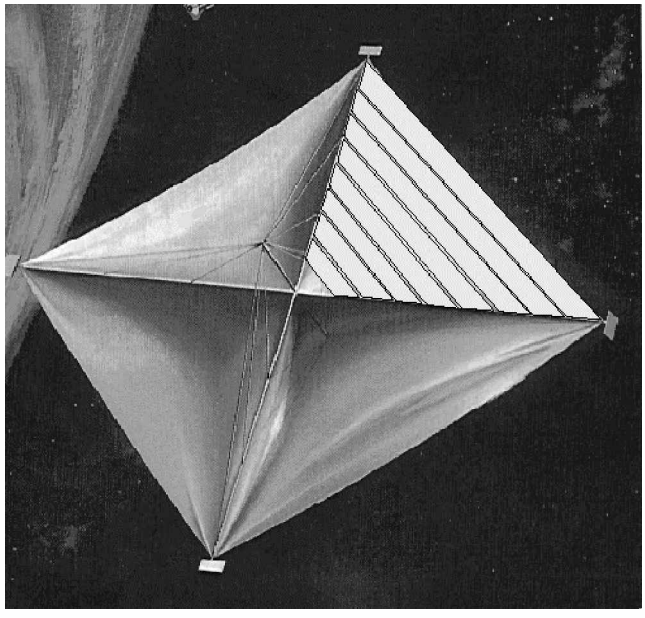

Fig. 4 Stripped architecture on one quadrant, based on the cover of Ref. 3.

Table 1 Boom load prediction errors for ignored catenary slope tangents (expressions c and d, Fig. 5)

	Error (%) for ξ:			
Expression	0.025	0.05	0.10	0.15
c	−9	−16	−26	−34
d	−4	−7.5	−13	−18

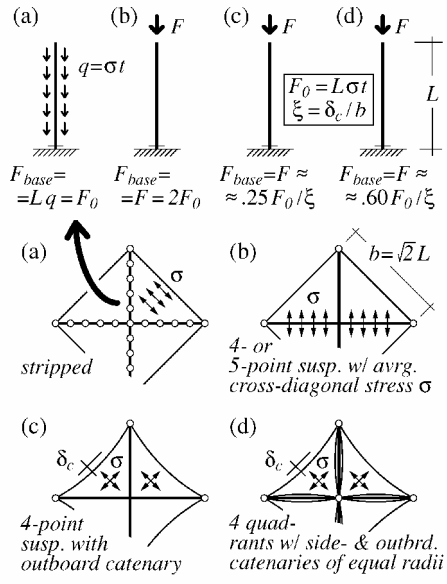

Fig. 5 Boom axial forces for four designs.

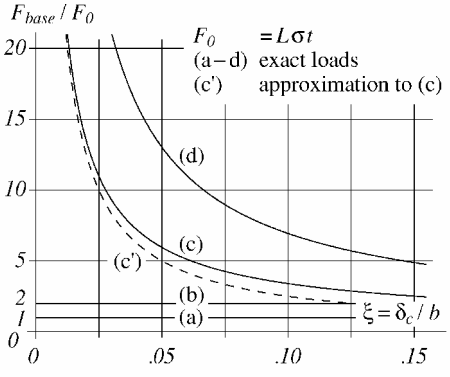

Fig. 6 Boom load vs outboard catenary sag, Fig. 5.

the boom load predictions themselves, depend little on whether the catenary shape is correctly considered circular or assumed parabolic.

The exact boom loads for the designs in Figs. 5a–5d, along with the approximation shown there for the case, Fig. 5c, are plotted in terms of the normalized outboard catenary sag $\xi = \delta_c/b$ in Fig. 6. (Figure 5c derives from an assumed parabolic catenary shape via ignoring catenary end slopes.) Clearly, catenaries, curves c and d (Fig. 6), carry a heavy load penalty, especially in the likely range of interest, $\xi < 0.05$. The stripped design a corresponds to the lowest loads. The nonconservative error of the approximate expression, curve c′, is also apparent.

Beyond the lowest boom compression, the stripped design also possesses the most favorable load distribution (Fig. 5). Still, the upper bound nature of this scheme cannot yet be claimed with absolute certainty for two reasons. First the relative magnitude of the film stresses for smoothness for uni- and biaxial tension (here assumed equal, σ) has not been rationally established. Second, sail suspension may favorably alter the nature of boom loading. For example, boom compression acquires some follower characteristics if a bidirectionally stretched sail is attached to the boom at several points (Fig. 1d).

The uniaxial tension in the stripped sail creates a tension field in membrane analysis terminology.[6] As alluded to earlier, we assume that transverse wrinkling, common in tension fields, can be controlled without significant transverse stressing.

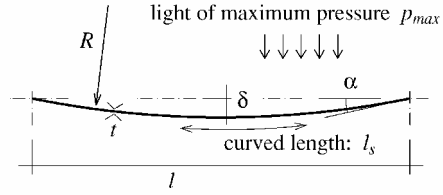

Fig. 7 Strip billow.

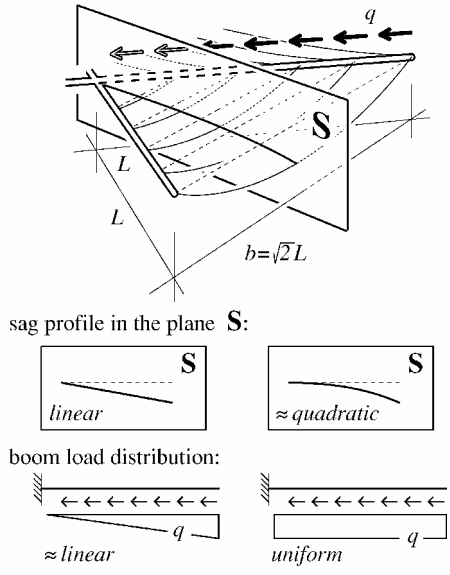

Fig. 8 Billow profile defines the boom loads.

Beyond its upper bound nature, the stripped design also simplifies the complex sail billow problem. The uniaxial tension state makes the sail surface equivalent to a set of strips (interconnected or not), the δ billow of each independently developing as if in two dimensions (Fig. 7). This deterministic behavior makes sail sag analysis rational and reliable, allowing billow to be easily designed into the sail. Thus, nonlinear and sensitivity issues, associated with a sail matching its suspension, are easily avoided. By engineering sag across the surface, one can design the load distribution on the booms as described next.

Boom Load Distribution vs Strip Billow Profile

The sail strip billow shape (Fig. 7) is not trivial due to the nonuniformity of the surface light pressure according to the cosine-square law (Wright,[3] Fig. 1.1) and inertial loads. Yet it can be well approximated with either a circular arc or a parabola if sufficiently shallow $\delta/l \ll 1$, the range of current interest. Thus, for illustrative purposes, assumptions related to these two shapes are used hereafter. (However, the program SqS used for the design study relies only on the parabolic approximation because the errors associated with this assumption can be seen to work in opposite directions, thus reducing one another. This is not so for the arc shape.)

When the variations along the strip of the billow radius of curvature R and of the effective surface pressure p are ignored, the strip membrane force $N = \sigma t$ linearly relates to R:

$$N = \sigma t = Rp \tag{1}$$

When the billow slope is ignored further, the local value q of the distributed boom axial load by the strips on both sides of the boom becomes, using Eq. (1),

$$q = N = Rp \tag{2}$$

(Contrary to the catenary end slopes discussed earlier, the strip slope ignored here is not critical in a reasonable design.) This linear dependence of q on the local strip curvature enables one to define the boom loads via R, or, equivalently, via the sag δ that determines R. In other words, the boom loads can be tailored via the sag profile

(the sag distribution across the sail surface) (Fig. 8). To achieve a particular boom load distribution, the sag profile has to be engineered into the sail. For uniform boom loading, the sag has to vary near quadratically from the sail center out.

The minimum film stress requirement $\sigma \geq \sigma_{\min}$ for smoothness and the limitations of fabrication technology $t > t_{\min}$ severely limit the permissible billow curvature

$$R > R_{\min} = \sigma_{\min} t_{\min} / p \tag{3}$$

and the associated sag. This impacts how desirable sags can be achieved, as described next.

Constant Force Sail Suspension

Film Billows and Technological Tolerances

Examine the consequences of Eq. (3) for a sail at 1 astronomical unit (AU). Assume a typical $\eta = 0.85$ effective specular reflective efficiency and $\sigma = \sigma_{\min} = 1$ psi skin stress. To relax the constraint imposed on R by Eq. (3) as much as possible, maximize solar light pressure to $p = \eta p_0 = 0.85 \times 9.126\ \mu\text{Pa} = 7.757\ \mu\text{Pa}$ by orienting the sail to face the sun.

The limit shapes $R = R_{\min}$ satisfying Eq. (3) for these conditions are here characterized via the billow strain, the relative length difference between the curved strip l_s and the span l: $\varepsilon_{\text{billow}} = (l_s - l)/l$ (cf. Fig. 7). A deformed strip (sag) geometry is effectively defined by $\varepsilon_{\text{billow}}$ for any given sag shape (circular arc, parabola, or other).

The lower $\varepsilon_{\text{billow}}$, the is greater R: the lower bound $R_{\min}$ on R according to Eq. (3) corresponds to an upper bound on $\varepsilon_{\text{billow}}$. The limit $\varepsilon_{\text{billow}}$ values consequently calculated for the adopted conditions are shown in Fig. 9 for three film thicknesses for parabolic sag. The strains are very low: Even for the upper end of the range shown at $l = 100$ m, they rapidly drop with nearly two orders of magnitude from about $\varepsilon_{\text{billow}} \approx 5E{-}4$ for a $t = 0.04$ mil $\approx 1\ \mu$m film as t increases to 0.25 mil with a factor slightly greater than six. The lowest value shown, for $l = 4$ m span, is near $\varepsilon_{\text{billow}} = 1E{-}8$. For proper sail operation, billow strains this small should be provided robustly and with sufficient accuracy. (Raising or lowering billow strain from the target value would quickly lower or increase film tension, leading to insufficient film stress or overstressing.)

For bidirectional film stressing, to which Eq. (3) does not directly apply, R (equivalently, $\varepsilon_{\text{billow}}$) in any particular direction corresponds to a perceived fraction of p (to $p/2$ for an isotropic stress state). Thus, the billow strains are even more severe than in Fig. 9.

Deformations from structural imperfections, thermal effects, fabrication tolerances, film crease set, etc., are significantly greater than those required for proper operation and shown in Fig. 9. Billow geometry to match these numbers cannot be engineered by sufficiently exact geometric design and fabrication, but has to be addressed indirectly. One practicable approach may be using a constant force sail suspension mechanism, which directly and robustly provides the skin stress required for surface smoothness and allows the sag to automatically adjust to the loads, environment, and structural imperfections. Such a fault-tolerant system influences how sail structures operate and fail as follows.

Sail Response, Failure, and Constant Force Suspension

If a constant force sail suspension is used, boom compression and sail tension decouple from solar loads, thermal effects, and structural imperfections. High fault tolerance results: structural damage due to overloading is eliminated. Beyond the operational state, this

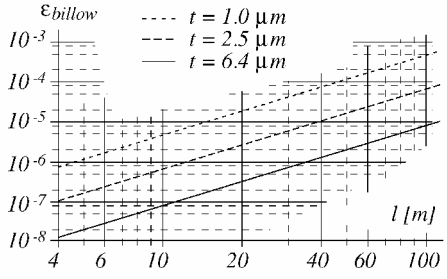

Fig. 9 Billow strain vs strip span l for $\sigma = 1$ psi, skin stress at 1 AU, and $\eta = 0.85$ (assumed parabolic billow shape).

Table 2 Responses for constant force sail suspension

Condition	Response
Excessive effective light load (too near to sun or too much payload).	Billows and boom lateral loads increase. Film tension and boom compression remain.
Light load too low (diversion from the sun).	Billows and boom lateral loads drop. Film tension and boom compression remain.
Dynamics (attitude control, orbital, and postdeployment effects).	Member load spikes and damage alleviated. Vibration frequency drops.
Curved sail deployment lock (umbrella turn-out).	Overloading avoided and deadlock may be bypassed.
Sail/boom dimension errors (fabrication errors and temperature loads).	Suspension stroke absorbs kinematic load. Sail tension, billow, and boom loads remain.
Lateral boom shape errors (fabrication errors and temperature loads).	Overstressing is avoided in designs where this could otherwise be a concern.

may also benefit deployment robustness by defusing a key component of the mechanism that can lock some structures in an erroneous kinked state if deployment goes astray. The cost of these benefits is a lower stiffness manifest in low natural frequencies and in a lack of effective boom lateral support by the film sheet. Table 2 summarizes some possibly critical loading and environmental conditions for sail operation and safety and how constant force sail suspension impacts the associated structural response. Solar, environmental, and kinematic disturbances are included.

To realize the preceding benefits robustly, sufficient stroke should be provided for the constant force suspension. If the stroke is exhausted by a part of the loads, the response stiffens for the remaining loads: The response characteristics change en route. To engineer such a scenario requires a nonlinear approach.

Note that a curved boom responds to compression as a near-constant force spring. In principle, therefore, it can replace or augment actual constant force springs.

Engineering Convenience for the Stripped Design

For a stripped sail, one is likely to use the same constant force spring parameters along the booms. Accordingly, stripped sail boom loading is taken uniform (Fig. 5).

Limit Point Friendly Design

Structural stability phenomena are generally avoided by design with a wide margin because 1) strength may drop dramatically at buckling, 2) loss of stability may cause unpredictable or violent response, and 3) near-limit load sensitivity to imperfections and disturbances may be unacceptable and is difficult to reliably model with simple tools. It is next seen that only the last of these points matters in the context of the global stability of sail booms with no rigs. Consequently, no safety concerns preclude adopting a limit point friendly design approach.

Strength Drop

The loss of global stability of a (tapered or uniform) boom corresponds to a loss of lateral stiffness, but not to a drop in the supported axial force; the axial stiffness disappears neither at nor beyond the Euler load. This is illustrated by the lateral and axial tip deflections of a uniform boom shown in Fig. 10 (dashed curves), generated by numerically solving the classic elastica problem. Clearly, load bearing capacity continues to increase, albeit modestly, after buckling. This renders the concern of postbuckling strength drop irrelevant.

Column vs Nonlinear Beam-Column Response

Because global buckling is not accompanied by a drop of load bearing capacity, no load suddenly remains unsupported when the event occurs: Reconfiguration into the buckled state can be quasi static. For a solar sail boom in the operating condition, even the direction of deformations is well defined by the lateral light pressure. This small load both 1) biases the structure to lean in one direction and 2) eliminates the buckling phenomenon by transforming the boom into a beam column.[7] Recall this transformation with a boom

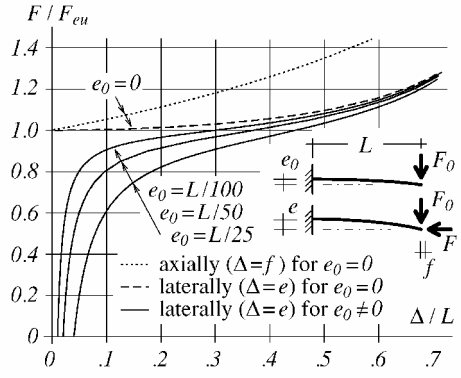

Fig. 10 Beam-column ($e_0 \neq 0$) vs column ($e_0 = 0$) response.

model subject to F_0 lateral tip loads of a range representative of the solar pressure load for a sail boom (Fig. 10, continuous lines).

A beam column does not buckle when the Euler load is passed: It simply continues to follow a soft deformation path characterized by plot(s) somewhat similar to the Euler response. However, this similarity can be rather stretched in sufficiently slender booms. The considered response of such members exhibits none of the unpredictable or violent characteristics of buckling phenomena that necessitate safeguarding structural integrity by avoiding the stability limit.

Embracing Compliance in Design

Near the Euler load, column and beam-column response are sensitive to even minor disturbances (cf. Fig. 10). This sensitivity is accepted here via the assumption that future gossamer space structure design will not eliminate such compliance by default, but will examine first whether the weight penalty of elimination is justified. Therefore, with acknowledgment that no strength-related reason renders approaching the Euler load of a cantilever boom inherently dangerous, it is decided to 1) specify no margin of safety against Euler buckling and 2) adopt nonlinear beam-column analysis for the reliable modeling of sail booms.

By its general scope and rationality, this approach enables or facilitates 1) the accurate study of near- and postbuckling response; 2) sensitivity studies; 3) any boom construction, taper, and loading; and 4) curved booms for shaped (nonflat) sails for passive attitude control or other reasons. For the present project, nonlinear beam-column analysis was implemented in the two first-generation spreadsheet programs, SqS and Elastica. Both programs involve sophisticated numerics for the automatic execution of boom shape integration and the calculation of loads that depend on the boom deformations, embedded in a global iteration loop controlled by the user. Further comments on selected aspects of the nonlinear beam-column analysis of sail booms follow.

Real-Life Conditions

Environmental loads and fabrication errors may disturb a boom more than solar pressure, absorbing the effects of the latter. To assess such phenomena, nonlinear beam-column analysis is needed even if no solar loads are present. That a boom remains to deflect in a desired direction may have to be ensured with engineering measures.

Balanced Disturbances

Some boom disturbances (light pressure, gravity gradient and thermal loads, etc.) depend on sail orientation. Therefore, orientations where disturbances balance may exist. When this happens, the boom lateral deformations either disappear, if the axial load is below the Euler load, or maintain their earlier direction. Deformation assessment and management in such cases needs to involve sensitivity studies, which cannot be rationally performed without nonlinear beam-column analysis.

Design for Euler Buckling

The scope of beam-column analysis includes classic Euler buckling: It yields the initially perfect column shape for compression with less than the Euler load and predicts the postbuckling response otherwise. Therefore, it can also be used to verify designs against Euler buckling.

Local Buckling

A global beam-column analysis must be validated by checking the booms against local wall (component) buckling. This is automatically performed in SqS and Elastica for tubular booms.

Rigged Booms

Rigs may suppress boom deformations effectively enough to render linear analysis acceptable, provided that imperfections and environmental deformations are controlled. In such cases, one can design the boom segments between rig attachment points with the traditional approach and focus on Euler buckling.

Design Study

By the use of the stripped architecture and the nonlinear analysis methodology discussed, a parametric design study has been performed to 1) demonstrate these innovations, 2) contribute toward exploring the achievable ultimate performance of square sails with unrigged booms, 3) provide point designs, and 4) map how variations of some design conditions affect achievable performance. The effort focused on 100-m sails, likely targets for near- to medium-term development efforts. Four baseline designs in this class, with different boom wall thicknesses, were established and then repeatedly redesigned with some of the design conditions altered.

All designs were optimized. The basis of optimization was the characteristic acceleration a_c imparted to the craft by sunlight at 1 AU. This natural measure rates the true compound efficiency of a sailcraft and can be directly used in mission design.[3] It is not only the structural design parameters that define a_c, but also all aspects of sailcraft assembly, position, orientation, and member responses, including the payload mass, film reflectivity, member deformations, and various nonlinearities. The latter include the dependence of structural loads on component (film, boom, payload, etc.) masses, as well as geometric nonlinearities due to the coupling of the loads with the boom deformations.

The accuracy of the calculated characteristic acceleration a_c depends on how well the propulsive force and the sailcraft mass are assessed. In the design program SqS, both are based on the actual deformed and billowed configuration geometry in the design conditions. The mass includes the actual sail mass integrated across the curved surface deformed into the designed billow.

Propulsion is calculated from the spatially deformed sail geometry with the cosine cube law, derived for configurations where the direction of acceleration coincides with that of the propelling light (the case for the symmetric sails directly facing the sun considered here). According to this relation, the component of the light pressure in the direction of the sail acceleration (the propulsive pressure p_p) is

$$p_p = p_0 \cos^3 \theta \tag{4}$$

with θ the angle between the surface normal and the direction of incident light (cf. Wright,[3] Fig. 1.1) and p_0 the surface light pressure if $\theta = 0$. Integrating p_p over the curved sail surface gives the total propulsive force.

Baseline Designs

The following conditions (default for the parametric design study) strictly hold for all four baseline sails:

1) The four booms lock into a hub of $r_h = 5$ cm radius.

2) The boom lengths, invariable during design optimization, derive from the nominal flat sail size b and the hub radius. (The actual sail size and shape depend on the deformed boom shapes in the design state.)

3) The nominal sail square edge is $b = 100$ m.

4) The payload mass is $m = 20$ kg, and a 2.5-kg mechanical overhead is present. Both are located at the center hub.

5) The sail accelerates from a circular orbit directly facing the sun at 1 AU.

6) The component of light pressure tangential to the film surface is negligible.

7) The sail is a stripped design, with a $\sigma = 1$ psi $= 6895$ Pa skin stress required for wrinkle control.

Table 3 Optimization of 100-m baseline designs A–D

Parameter	Value				
	Boom wall thickness $t_b = 0.10$ mm = 4 mils				
d, cm	7.62	7.11	6.96	6.91	6.86
EI, Nm^2	1217	989.6	927.3	907.2	887.3
ρ_l, g/m	40.4	37.7	36.9	36.6	36.3
z_{tip}, m	1.057	2.325	3.474	3.821	5.085
a_c, mm/s^2	1.019	1.025	1.022	1.020	1.011
m_{tot}, kg	76.08	75.33	75.13	75.14	75.02
m_{4b}, kg	11.41	10.65	10.42	10.35	10.27
m_{4b}/m_{film}	0.271	0.253	0.247	0.245	0.277
R_{Eu}	1.54	1.26	1.18	1.15	1.13
Comment	——	Design A	——	——	Not unique
	Boom wall thickness $t_b = 0.15$ mm = 6 mils				
d, cm	7.11	6.60	6.10	6.07	6.05
EI, Nm^2	1484	1188	934.8	923.1	911.6
ρ_l, g/m	56.5	52.5	48.5	48.2	48.1
z_{tip}, m	0.641	1.131	3.255	3.571	50.77
a_c, mm/s^2	0.962	0.975	0.980	0.979	0.090
m_{tot}, kg	80.64	79.50	78.39	78.35	76.38
m_{4b}, kg	15.98	14.84	13.69	13.64	13.58
m_{4b}/m_{film}	0.379	0.352	0.325	0.323	0.337
R_{Eu}	1.88	1.51	1.19	1.17	1.16
Comment	——	——	Design B	——	Unsound
	Boom wall thickness $t_b = 0.20$ mm = 8 mils				
d, cm	6.10	5.59	5.54	5.51	5.49
EI, Nm^2	1246	960.0	934.1	921.3	908.6
ρ_l, g/m	64.6	59.2	58.7	58.4	58.1
z_{tip}, m	0.981	2.703	3.266	3.612	51.51
a_c, mm/s^2	0.935	0.947	0.946	0.944	0.080
m_{tot}, kg	82.93	81.43	81.29	81.22	78.73
m_{4b}, kg	18.26	16.74	16.58	16.51	16.43
m_{4b}/m_{film}	0.433	0.397	0.393	0.392	0.417
R_{Eu}	1.58	1.22	1.18	1.17	1.15
Comment	——	Design C	——	——	Unsound
	Boom wall thickness $t_b = 0.25$ mm = 10 mils				
d, cm	5.59	5.08	5.03	5.00	4.98
EI, Nm^2	1200	901.6	874.8	861.6	848.6
ρ_l, g/m	74.0	67.3	66.6	66.3	65.9
z_{tip}, m	1.092	4.312	5.938	7.396	56.98
a_c, mm/s^2	0.905	0.911	0.900	0.885	0.045
m_{tot}, kg	85.59	83.75	83.61	83.58	75.59
m_{4b}, kg	20.92	19.02	18.83	18.73	18.64
m_{4b}/m_{film}	0.497	0.451	0.446	0.443	0.542
R_{Eu}	1.52	1.14	1.11	1.09	1.08
Comment	——	Design D	——	——	Unsound

8) Sail film thickness is $t = 2.5\ \mu\text{m} = 0.1$ mil.

9) The film suffers a 0.1% crease set in stowage.

10) The effective efficiency of specular reflectivity is $\eta = 0.85$ regardless of film tension and other conditions, a number where all effects influencing reflectance are lumped, including how well wavelike soft wrinkles are controlled. This number is lower than the $\eta_{\max} = 0.9$ considered the achievable maximum.[3]

11) The booms are tubular.

12) The boom wall Young's modulus and Poisson's ratio are $E = 68.95$ GPa $= 10 \times 10^6$ psi and $\nu = 0.3$.

13) The boom wall and sail film material volume densities are $\rho = 1660$ kg/m^3 (this corresponds to a specific weight of $\gamma = 0.060$ lbf/in.^{3} at sea level).

The baseline designs, denoted A–D hereafter, have been optimized for these conditions with $t_b = 0.10, 0.15, 0.20$, and 0.25 mm (4, 6, 8, and 10 mils) tube wall thicknesses. These designs and some alternatives (proved inferior during optimization) are shown in Table 3 via the cross section diameter d, flexural stiffness EI, and linear density ρ_l. The boom response in the design state is characterized with the tip deflection z_{tip}. The entire sailcraft mass m_{tot}, the total mass of the booms m_{4b}, and the structural mass fraction m_{4b}/m_{film} are also given. The characteristic acceleration a_c reveals performance. Finally, the margin of safety against global buckling R_{Eu} helps relate each design to traditional conditions. The Euler buckling load for the calculation of R_{Eu} was, for the current uniformly distributed load pattern Fig. 5a, obtained via the formula

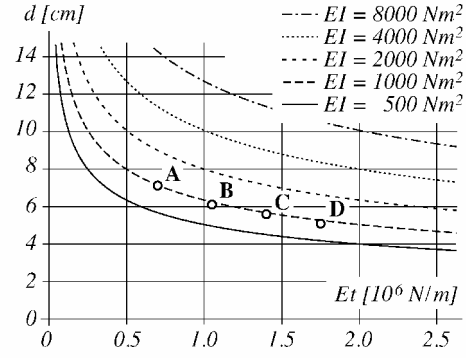

Fig. 11 Cross section diameter d vs wall stiffness Et and bending stiffness EI; points A–D mark the $b = 100$ m baseline designs; Table 3.

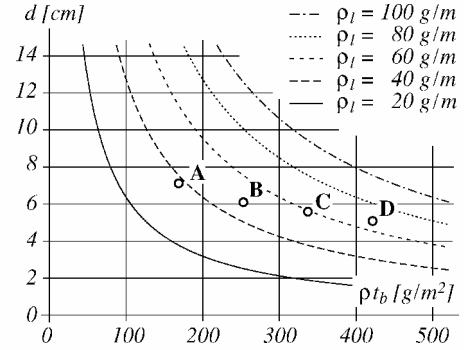

Fig. 12 Cross section diameter d vs boom wall surface density ρt_b and linear density ρ_l; points A–D mark the $b = 100$ m baseline designs; Table 3.

$$q_{\text{cr}} = 7.837EI/L^3 \tag{5}$$

from Timoshenko.[8]

The baseline designs A–D are marked in the comment lines. The cases with excessively deformed booms and low performance, marked unsound, highlight the limitations of the engineering effort. These designs correspond to conditions (diameters d) that, for practical purposes, proved incompatible with the constraints (specifications) spelled out earlier. The last design for wall thickness $t_b = 0.1$ mm is marked not unique because the conditions that define this configuration are also compatible with another (unsound) design geometry, not shown.

The boom cross section properties for the best (the baseline) designs are remarkably similar for all wall thicknesses. Cross section flexural stiffness is nearly constant, whereas the variation of boom linear densities is modest (Figs. 11 and 12).

The following practically significant observations are drawn directly from the tabulated data:

1) The design optima A–D correspond to low Euler buckling margins $R_{\text{Eu}} = 1.14$–1.26.

2) Optimal performance is not degraded dramatically by slight to moderate boom cross section variations.

3) The structural mass fraction m_{4b}/m_{film} does not reflect performance well; it continues to drop consistently with the boom dimensions even after the design optimum is passed.

4) Best performance corresponds to deformations small enough to permit linear boom design. (However, a linear approach cannot address nonlinear sensitivities significant in slender booms, and it undershoots deformations. Underestimated deflections lead to overestimating propulsion, a nonconservative error.)

Typical parameter ranges for the baseline designs have been reviewed in Fig. 2 in the Introduction.

The Need for the Right Design Approach

To illuminate the need for the right design approach, the baseline booms have been placed in two differently defined design contexts: 1) linear boom modeling and 2) a static sailcraft model where the inertial effects of the acceleration by the light are not accounted for. Linear boom analysis was performed by disabling the nonlinear

Table 4 Deformed design geometries and performance with the baseline booms A–D, $b = 100$ m, based on linear boom design and under an altered condition

	Configuration			
Parameter	A	B	C	D
d, cm	7.11	6.10	5.59	5.08
t_b, mm	0.10	0.15	0.20	0.25
	Designs based on linear approximations			
z_{tip}, m	0.446	0.470	0.457	0.485
a_c, mm/s^2	1.030	0.990	0.953	0.927
	Regular (nonlinear) designs with 500-kg carrier			
z_{tip}, m	6.128	8.597	7.225	11.77
a_c, mm/s^2	0.0131	0.0126	0.0128	0.0118

Table 5 Designs with boom taper, $b = 100$ m

	t_b, mm			
Parameter	0.10	0.15	0.20	0.25
d_{base}, cm	10.2	9.14	8.89	8.13
d_{tip}, cm	1.27	1.02	0.762	0.610
EI_{base}, Nm^2	2885	3155	3866	3693
EI_{tip}, Nm^2	5.64	4.33	2.43	1.56
$\rho_{l,\text{base}}$, g/m	53.6	72.7	94.2	107.7
$\rho_{l,\text{tip}}$, g/m	6.73	8.08	8.08	8.08
z_{tip}, m	1.696	1.454	1.035	1.335
a_c, mm/s^2	1.015	1.016	0.979	0.955
m_{tot}, kg	73.25	76.09	79.13	81.04
m_{4b}, kg	8.56	11.41	14.46	16.94
m_{4b}/m_{film}	0.203	0.271	0.343	0.402

aspects of the beam-column sections of SqS. Static analysis was carried out by attaching a large (500-kg) mass to the sail to suppress acceleration by light pressure, equivalent to the state when the sail is docked to a carrier. The optimal sail design geometries associated with these altered conditions are indicated in Table 4 by the boom deflections. Characteristic accelerations a_c are also given.

Comparison with Table 3 reveals the following: 1) Ignoring the nonlinear aspect of boom deformations results in undershooting displacements with a factor of five to eight. 2) Not accounting for the acceleration by light (equivalent to designing for the docked, as opposed to the flight, state) entails two to three times greater deformations than otherwise.

Parametric Study

To study the sensitivity of performance and some structural parameters to design conditions and assumptions, some of the default specifications were individually varied and the sails redesigned.

Boom Taper

A linear taper of the boom radii was allowed. Optimization by varying the base and tip radii yielded the designs in Table 5. Comparing the results with Table 3, one observes that the performance (a_c) improved only slightly. This may be due to two reasons. First, the achieved 10–20% boom mass reduction is small compared to the total mass m_{tot}. Second, the cosine cube law [Eq. (4)] results in a loss of propulsion for tapered booms near the sail edge where the deflection of the slender tapered boom tips make the sail canopy steeper. This deformation pattern was noted on the boom shapes (not shown) despite the reduction of the boom tip deflections (z_{tip}, see tables). Taper reduces boom deformations in the sail interior, but it intensifies boom tip curvature.

Taper effects have also been examined for the other conditions studied (Tables 6–9). These further results generally support the preceding observations.

Sail Size

To assess how performance scales, the sail size was increased to $b = 400$ m and the center hub radius to 20 cm. Accordingly, the 20-kg baseline payload and 2.5-kg mass overhead were changed to 320 and 10 kg, respectively. The optimal designs for these conditions are shown in Table 6 for both uniform and tapered booms.

Table 6 Designs for $b = 400$ m sails

	t_b, mm			
Parameter	0.10	0.15	0.20	0.25
	Without taper			
d, cm	30.7	26.7	24.1	22.1
EI, Nm^2	79860	78280	77300	74210
ρ_l, g/m	162.8	212.0	255.7	292.7
z_{tip}, m	14.80	15.62	16.17	18.27
a_c, mm/s^2	1.031	0.984	0.945	0.912
m_{tot}, kg	1190	1245	1295	1337
m_{4b}, kg	184.1	239.6	289.1	330.9
m_{4b}/m_{film}	0.273	0.355	0.428	0.490
R_{Eu}	1.58	1.55	1.53	1.48
	With taper			
d_{base}, cm	42.4	36.6	33.5	31.0
d_{tip}, cm	7.11	6.35	5.59	4.83
EI_{base}, Nm^2	21000	20190	20740	20460
EI_{tip}, Nm^2	989.6	1057	960.0	773.0
$\rho_{l,\text{base}}$, g/m	225	291	355	411
$\rho_{l,\text{tip}}$, g/m	37.7	50.5	59.2	63.9
z_{tip}, m	12.71	13.83	13.75	15.33
a_c, mm/s^2	1.062	1.020	0.986	0.956
m_{tot}, kg	1154.2	1198.9	1240.4	1274.6
m_{4b}, kg	148.4	192.9	234.3	268.2
m_{4b}/m_{film}	0.220	0.286	0.347	0.397

Table 7 Sail film, $t = 1.0$ μm $= 0.04$ mil, 100-m designs

	t_b, mm			
Parameter	0.10	0.15	0.20	0.25
	Without taper			
d, cm	5.72	4.90	4.42	4.06
EI, Nm^2	513.5	486.1	475.0	461.6
ρ_l, g/m	30.28	38.96	46.83	53.83
z_{tip}, m	3.460	3.943	4.154	4.477
a_c, mm/s^2	1.601	1.518	1.452	1.396
m_{tot}, kg	47.94	50.40	52.63	54.61
m_{4b}, kg	8.559	11.01	13.24	15.22
m_{4b}/m_{film}	0.507	0.653	0.785	0.902
R_{Eu}	1.63	1.54	1.51	1.46
	With taper			
d_{base}, cm	8.89	6.35	——	——
d_{tip}, cm	0.762	1.14	——	——
EI_{base}, Nm^2	1933	1057	——	——
EI_{tip}, Nm^2	1.217	6.162	——	——
$\rho_{l,\text{base}}$, g/m	47.10	50.47	——	——
$\rho_{l,\text{tip}}$, g/m	4.037	9.084	——	——
z_{tip}, m	2.210	5.334	——	——
a_c, mm/s^2	1.652	1.565	——	——
m_{tot}, kg	46.61	47.86	——	——
m_{4b}, kg	7.227	8.416	——	——
m_{4b}/m_{film}	0.428	0.497	——	——

Apparently, performance and some other parameters (e.g., the structural mass fractions m_{4b}/m_{film}) are barely affected by the scaling. However, the Euler margins R_{Eu} (presented for reference, not for relevance to design efficiency or safety) increased notably. Taper, again, failed to improve the designs significantly.

A difference between the $b = 100$ and 400 m designs is the significance of local buckling. Although this condition drove none of the optimal designs, it governed more nonoptimal designs for large sails than in the baseline case.

Key parameter ranges for the designs with uniform booms are shown in Fig. 3 in the Introduction.

Sail Film Thickness

The sail film thickness was then increased and decreased to $t = 1.0$ μm $= 0.04$ mil and 6.4 μm $= 0.25$ mil. All other design specifications remained. The performance of the resulting designs, shown in Tables 7 and 8 for both uniform and tapered booms,

Table 8 Sail film, $t = 6.4\ \mu m = 0.25$ mil, 100-m designs

	t_b, mm			
Parameter	0.10	0.15	0.20	0.25
	Without taper			
d, cm	9.27	8.13	7.26	3.38
EI, Nm^2	2192	2216	2109	2121
ρ_l, g/m	49.12	64.60	76.98	89.50
z_{tip}, m	1.273	2.153	2.312	2.127
a_c, mm/s^2	0.546	0.530	0.516	0.504
m_{tot}, kg	141.8	146.2	149.7	153.2
m_{4b}, kg	13.88	18.26	21.76	25.30
m_{4b}/m_{film}	0.132	0.173	0.207	0.240
R_{Eu}	1.11	1.12	1.07	1.08
	With taper			
d_{base}, cm	13.2	11.4	10.7	10.2
d_{tip}, cm	1.52	1.27	0.889	0.660
EI_{base}, Nm^2	6338	6162	6680	7213
EI_{tip}, Nm^2	9.737	8.452	3.866	1.981
$\rho_{l,base}$, g/m	69.98	90.84	113.0	134.6
$\rho_{l,tip}$, g/m	8.075	10.09	9.421	8.748
z_{tip}, m	0.862	1.273	1.456	1.395
a_c, mm/s^2	0.558	0.544	0.532	0.522
m_{tot}, kg	139.0	142.2	145.3	148.2
m_{4b}, kg	11.03	14.26	17.31	20.26
m_{4b}/m_{film}	0.105	0.135	0.164	0.192

Table 9 $E = 137.9$ GPa $= 20 \times 10^6$ psi, 100-m designs

	t_b, mm			
Parameter	0.10	0.15	0.20	0.25
	Without taper			
d, cm	5.72	4.95	4.47	4.11
EI, Nm^2	1027	1003	983.0	958.3
ρ_l, g/m	30.3	39.4	47.4	54.5
z_{tip}, m	1.948	2.173	2.400	2.769
a_c, mm/s^2	1.056	1.019	0.989	0.962
m_{tot}, kg	73.24	75.81	78.07	80.10
m_{4b}, kg	8.559	11.13	13.39	15.41
m_{4b}/m_{film}	0.203	0.264	0.318	0.366
R_{Eu}	1.30	1.27	1.25	1.22
	With taper			
d_{base}, cm	7.87	6.60	6.10	5.84
d_{tip}, cm	1.14	1.22	1.07	0.711
EI_{base}, Nm^2	2686	2377	2493	2742
EI_{tip}, Nm^2	8.22	15.0	13.4	4.95
$\rho_{l,base}$, g/m	41.7	52.5	64.6	77.4
$\rho_{l,tip}$, g/m	4.07	9.69	11.3	9.42
z_{tip}, m	1.803	2.110	1.907	2.254
a_c, mm/s^2	1.081	1.050	1.024	1.001
m_{tot}, kg	71.44	73.48	75.42	76.98
m_{4b}, kg	6.75	8.79	10.73	12.27
m_{4b}/m_{film}	0.160	0.208	0.254	0.291

significantly differs from the baseline (Table 3). The last two columns, for 0.20- and 0.25-mm boom walls, are left blank for the thin film case (Table 7) because the associated tip cross section sizes dropped to impractical values during optimization. For these conditions, design optimum is defined primarily by boom fabrication technology.

Performance improves with 40–60% when the thinner film is used and drops 40–50% for the thick film. The change in the structural mass fraction m_{4b}/m_{film} is similarly marked. However, this change is inverse to the performance change, highlighting the parameter's limited value.

The margin R_{Eu} against the Euler load is also affected by the thickness: The thinner film corresponds to wider margins. However, the drop of R_{Eu} from the baseline designs for the thick film variants is much less significant.

Total sailcraft mass m_{tot} directly reflects film thickness. The performance improvement achieved by boom taper, although still not significant, is most noticeable for the thick film condition with thin boom walls.

Boom Material Stiffness

Optimal designs corresponding to a twofold increase of the boom wall Young's modulus to $E = 137.9$ GPa $= 20 \times 10^6$ psi are shown in Table 9. Performance improvement is generally modest, but gets more pronounced with the increase of the wall thickness. The Euler margins R_{Eu} are somewhat greater than the baseline. The boom deformations, on the other hand, drop up to 36% (0.25-mm wall) if no taper is used and slightly increase for tapered booms. The effect of taper on performance is, again, insignificant.

Achieved Performance

The designs generally achieve an $a_c \approx 0.9$–1 mm/s^2 characteristic acceleration and $\bar{\rho} \approx 5.3$–5.9 g/m^2 structural surface density regardless of boom taper, material stiffness, and sail size.

This efficiency could be effectively improved via the reduction of the sail film thickness (as seen) and/or of the payload (here arbitrarily assigned). Booms of better materials or of more efficient architectures[9] such as isogrid, coiled-longeron, or cable-and-spreader stiffened designs would have a limited effect in the baseline conditions because they do not dominate the total mass (m_{4b} vs m_{tot} in Tables 3–9). However, the booms could become the bottleneck for sufficiently low film thicknesses and payload masses.

Summary of Observations

The comparison of sail architectures and the study of general design issues (including sail billow) led to these conclusions:

1) Sail suspension should involve constant force mechanisms.

2) Constant force sail suspension positively affects response in many operational and failure modes.

3) Ignoring catenary end slopes may lead to serious nonconservative errors.

4) Catenaries heavily penalize design.

5) The stripped configuration has significant benefits, and it likely represents the ultimate achievable efficiency.

6) Nonlinear beam-column effects can be significant.

The list continues when it is noted that the parametric design study of various design conditions and assumptions revealed the following:

7) Good structural economy corresponds to small boom deformations.

8) Optimal design efficiency is not degraded dramatically by slight to moderate boom cross section variations.

9) Boom taper barely improves efficiency.

10) Ignoring nonlinear deformation effects may result in significantly underestimating displacements.

11) Ignoring inertial effects due to the propulsive acceleration (equivalently, design for a docked state) may entail two to three times greater boom deformations than the flight configuration.

12) Structural mass ratio measures performance poorly.

13) Efficiency is barely effected by sail size if the payload is scaled with the sail area.

Engineering

The focus of this paper is not to suggest technical solutions, but to guide future engineering by identifying key limitations and trends. Nevertheless, practical challenges and possible answers to these challenges were constantly debated during this project. Some of the issues considered are briefly mentioned here to add a dimension of hardware engineering to the present work and to contribute to the ongoing debate on gossamer technology.

Addressing concerns touched on in this paper (or some that are related to the issues here raised), one might consider, among other options: 1) providing constant force sail suspension conditions via crease patterns engineered into the sail film itself; 2) shape control via a) an engineered shape bias to overwhelm uncontrollable imperfections and b) an auxiliary system (rigs, cables, or other elements) to hold the structure at, or move it back to, the desired geometry; 3) the control of transverse wrinkles in uniaxially tensioned films by light lateral riblike stiffeners mounted on or integrated into the film; 4) realizing tubular booms with the well-known stem or bistem construction[10,11] or with rigidizable composite technology; 5) simplifying design and fabrication by avoiding sail edge catenaries regardless of film sheet shape—triangular, square, etc. (in

addition to the boom load penalty discussed earlier, catenaries also add weight, are expensive to robustly integrate onto the film, and entail film-cable deformation compatibility issues); and 6) reducing mass overhead by eliminating hardware elements not critical during the flight (detach or remove before free flight all components, motors, canisters, inflation bladders, pressurization devices, power- and force transmission elements such as chords, some stiffeners, etc., needed only for deployment).

Engineering for specific missions may involve the combination of low-weight technologies. For example, low-mass attitude control may be achieved by nanosatellites anchored to a sailcraft directly at boom tips, or with filaments or filament trusses, to 1) add leverage to the small device thrust, 2) increase system mass moment of inertia, or 3) add inertial drag to some structural locations.

Note also that the intuition gained by traditional structural engineering may be misleading in the realm of what gossamer engineering is or may one day become. Even some of the most fundamental design assumptions may be undermined. For example, the very concept of a static or quasi-static state may turn out to be superfluous: Dynamic responses to disturbances of very large and flexible structures may not damp out before newer disturbances (from attitude control, environmental effects, orbital dynamics, etc.) arise.

Future Work

Whereas the continuation of this work to step over some of its present limitations is a question of time only, overcoming some others requires the further development of the design software SqS. Maintaining flexibility and user-friendliness, SqS should be extended with the following features: 1) nontubular boom cross sections such as isogrid tubes and coilable longerons; 2) conventional sail architectures (requires basic research due to the billow problem involved); 3) the capability to subject designs to nondesign conditions (at the time of writing, SqS could only perform designs for one given set of conditions); 4) nonlinear models for film reflectance and response; 5) enhancements to aid mission design directly (asymmetric loads and boom loading, etc.); and 6) other enhancements, to be defined later.

Conclusions

A theoretical limit configuration of potentially maximum efficiency among like sails, the stripped architecture, was embraced to explore the limits of sail performance. This architecture, defined by uniaxial film tension in each sail quadrant parallel to the square sail edge, combines the advantages of 1) limited performance due to the absolute shortest load paths for film tensioning (collectively at all surface points) and 2) manageable billow mechanics. These characteristics enable reliable sailcraft analysis and design for the performance limit, here carried out with nonlinear beam-column boom analysis to 1) improve analysis reliability, 2) enable sensitivity studies, 3) permit structural flexibilities, and 4) allow near-limit point response. None of the designs discussed could have been rationally performed without nonlinear beam-column analysis.

The preceding innovations dramatically depart from the prevailing approach to square sail design, which often involves film suspension patterns with heavy load penalties and focuses on boom Euler buckling in the context of a linear analysis.

The safety of flexible booms with no required Euler margin was examined by reviewing design fundamentals. It was shown that, for straight booms under constant compression, neither does axial strength drop at Euler buckling, nor do violent responses occur. It was also seen that lateral disturbances as small as light pressure effectively transform slender sail booms into beam columns that do not buckle when the Euler load is passed, but follow a soft deformation path.

Finally, a design study with nonlinear beam-column analysis of the stripped architecture was performed to 1) contribute toward exploring the ultimate achievable performance of square sails, 2) demonstrate the proposed design approach, 3) provide point designs, and 4) map the impact of some design conditions on the achievable performance. Four baseline designs of different boom wall thicknesses were established and repeatedly redesigned with the boom taper, boom wall material stiffness, sail size, and film thickness varied.

This work was accomplished with SqS, a first-generation program for the fully nonlinear interactive design and analysis of square solar sails. To calculate properly the boom loads, SqS keeps track of the three-dimensional geometry of film strip billows and orientations as they depend on the curved boom shape.

All designs were optimized for maximum characteristic acceleration, a natural measure directly applicable to mission design. The cosine cube law, a practical relationship to calculate propulsion if the direction of the latter and of the incident light coincide, was introduced.

The designs generally achieved an $a_c \approx 0.9$–1 mm/s^2 characteristic acceleration and $\bar{\rho} \approx 5.3$–5.9 g/m^2 structural surface density regardless of boom taper, material stiffness, and sail size.

The theoretical considerations and the parametric design study have shown, among other observations, that 1) sails must be suspended with constant force mechanisms, 2) optimal designs correspond to small boom deformations, 3) sail performance is not dramatically sensitive to minor boom cross section variations in the vicinity of the optimum design; and 4) performance varies little in the 100–400 m size range.

Given that the design assumptions and conditions used have been specific and, to some extent, arbitrary, the conclusions should be extrapolated to other conditions with caution. The limiting aspects of the present work include, first, that only cylindrical cross sections have been examined—no isogrid or other structures (cable-stiffened, rigged, or coiled-longer) booms have been considered. Second, only the stripped design has been studied. Third, payload impact was not explored. (Payload mass affects sailcraft efficiency and how critical the boom design is for efficiency.) Finally, only one film skin stress value (6.9 kPa = 1 psi) has been considered. The scope of work should be expanded beyond these limitations in a more in-depth study.

Acknowledgments

This work has been supported by the NASA Langley Research Center, Hampton, Virginia; the U.S. Air Force Research Laboratory, Kirtland, New Mexico; and the NASA Jet Propulsion Laboratory, California Institute of Technology, Pasadena, California. It has been initiated and its focus on the stripped architecture initially defined by the second author, Martin Mikulas.

References

[1]Greschik, G., and Mikulas, M. M., "Solar Parachute Concept for Solar Power Satellites and Solar Sails," AIAA Paper 2000-1794, April 2000.

[2]McInnes, C. R., *Solar Sailing: Technology, Dynamics and Mission Applications*, 1st ed., Springer–Praxis Series in Space Science and Technology, Springer, London, 1999, published in association with Praxis, Chichester, England, U.K.

[3]Wright, J. L., *Space Sailing*, 1st ed., Gordon and Breach, Overseas Publishers Association, Amsterdam, 1992, p. 2.

[4]Harris, H. M., "Light Sails," *Scientific American*, Vol. 281, No. 2, 1999, pp. 90, 91.

[5]Leipold, M., Garner, C. E., Freeland, R., Herrmann, A., Noca, M., Pagel, G., Seboldt, W., Sprague, G., and Unckenbold, W., "ODISSEE—A Proposal for Demonstration of a Solar Sail in Earth Orbit," International Academy of Astronautics, Paper IAA.L98.1005, May 1998.

[6]Steigmann, D. J., "Tension Field Theory," *Proceedings of the Royal Society of London, Series A: Mathematical and Physical Sciences*, Vol. 429, No. 1876, 1990, pp. 141–173.

[7]Gaylord, E. H., Jr., Gaylord, C. N., and Stallmeyer, J. E., *Design of Steel Structures*, 3rd ed., McGraw–Hill, New York, 1992.

[8]Timoshenko, S. P., and Gere, J. M., *Theory of Elastic Stability*, 2nd ed., McGraw–Hill, New York, 1961, pp. 100–107.

[9]Mikulas, M. M., "Structural Efficiency of Long Lightly Loaded Truss and Isogrid Columns for Space Applications," NASA TM-78687, July 1978.

[10]MacNaughton, J. D., Weyman, J. D., and Groskopf, E., "The BI-STEM—A New Technique in Unfurlable Structures," *2nd Aerospace Mechanism Symposium*, edited by G. G. Herzl, NASA TM-33-355, 1967, pp. 369–375.

[11]Rimrott, F. P. J., "Storable Tubular Extendable Member," *Machine Design*, Vol. 37, No. 28, 1965, pp. 156–165.

C. Jenkins
Guest Editor